Western U.S. Infrasonic Catalog: Illuminating infrasonic hot spots with the USArray

Kristoffer T. Walker,[1] Richard Shelby,[1] Michael A. H. Hedlin,[1] Catherine de Groot-Hedlin,[1] and Frank Vernon[1]

Received 8 June 2011; revised 21 September 2011; accepted 27 September 2011; published 10 December 2011.

[1] In this study reverse time migration is applied to signals recorded by the 2007–08 USArray, presumably due to acoustic-to-seismic coupling, to detect and locate in two-dimensional space and time 901 sources of atmospheric infrasound, defining the Western United States Infrasonic Catalog (WUSIC). The detections are visually inspected and ranked. Uncertainties are estimated using a bootstrap technique. The method correctly locates most rocket motor detonations in Utah and a bolide explosion in Oregon with an average spatial accuracy of 50 km and 25 km, respectively. The origin time statistics for 2007 and 2008 events are nearly identical and suggest a predominant human origin. The event locations illuminate repeating sources of infrasound, or "infrasonic hot spots," in Nevada, Utah, and Idaho that are spatially associated with active military areas. The infrasonic arrivals comprise several branches that are observed to a range between 200 and 1500 km to the east and west of the epicenter in the winter and summer, respectively. The optimum group velocities are Gaussian distributed and centered at 295 m/s. A seasonal variation in optimum group velocities exhibits good correlation with atmospheric temperature. The results show that relatively dense seismic networks fill in the gaps between sparsely located infrasound arrays and provide valuable information for regional infrasonic source location and propagation studies. Specifically, the catalogs presented here can be used to statistically validate and improve propagation models, especially above the middle stratosphere where winds are not directly measured by ground-based weather stations or meteorological satellites.

Citation: Walker, K. T., R. Shelby, M. A. H. Hedlin, C. de Groot-Hedlin, and F. Vernon (2011), Western U.S. Infrasonic Catalog: Illuminating infrasonic hot spots with the USArray, *J. Geophys. Res.*, *116*, B12305, doi:10.1029/2011JB008579.

1. Introduction

[2] Atmospheric infrasound, acoustic energy with frequencies below ~20 Hz, travels across the globe at 200 to 400 m/s in relatively thin atmospheric ducts [e.g., *Landau and Lifshitz*, 1959; *Evers and Haak*, 2010, and references therein]. The heights of the ducts (typically in the stratosphere and lower thermosphere) depend on the effective sound speed, which is the sum of the static sound speed (a function of temperature) and wind speed in the propagation direction. Because atmospheric wind speeds can be a significant fraction of the static sound speed, the atmosphere can be highly anisotropic and form ducts in the direction of the prevailing winds [e.g., *Drob*, 2010]. The existence of these dynamic ducts often determines if one will observe an infrasonic signal at the Earth's surface [e.g., *Le Pichon et al.*, 2009; *de Groot-Hedlin et al.*, 2010, and references therein].

[3] The Comprehensive Nuclear-Test ban Treaty opened for signature in 1996. The Preparatory Commission for the Comprehensive Nuclear-Test Ban Treaty Organization (CTBTO) and the International Monitoring System (IMS), was formed shortly thereafter. The primary monitoring tool of the CTBTO, the IMS is a developing global network that will ultimately consist of seismic, hydroacoustic, radionuclide, and 60 infrasonic stations [e.g., *Christie and Campus*, 2010]. A typical infrasonic station (of the currently ~40 existing stations) comprises an array of several microbarometers with an aperture of 200 to 3,000 m. The average interstation spacing is 2,200 km. While recent studies suggest that this infrasound network is capable of realizing its design goal of detecting and locating a 1 kT or larger atmospheric explosion [*Le Pichon et al.*, 2009; *Green and Bowers*, 2010], the network is too sparse for careful investigation of many aspects of infrasonic propagation. Although relatively dense networks of regional infrasound arrays have provided new insights into propagation and detection patterns [e.g., *Le Pichon et al.*, 2008], a number of hypotheses or models still remain to be rigorously tested, including effective 4-D atmospheric velocity modeling approaches [e.g., *Drob et al.*, 2003; *Antier et al.*, 2007], thermospheric attenuation models [e.g., *Sutherland and Bass*, 2004; *de Groot-Hedlin et al.*,

[1]Institute of Geophysics and Planetary Physics, Scripps Institution of Oceanography, University of California, San Diego, La Jolla, California, USA.

0148-0227/11/2011JB008579

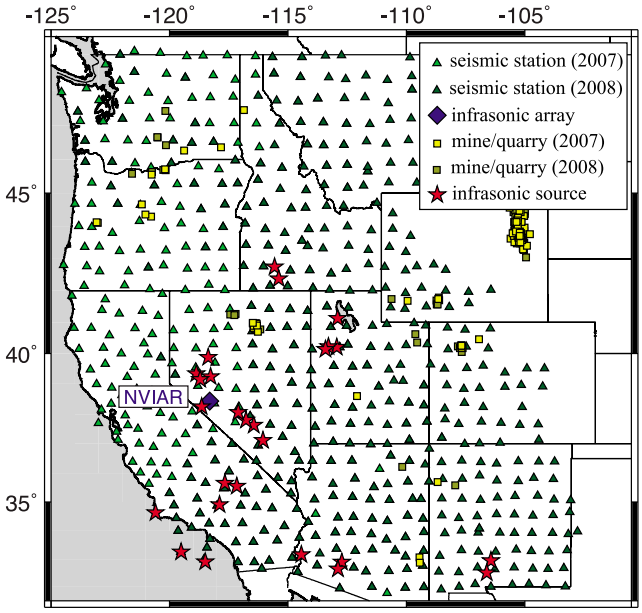

Figure 1. Location of USArray stations in 2007–08 with respect to potential infrasonic sources and the Nevada infrasound array NVIAR. Stars indicate military areas of potential infrasonic emissions that spatially correlate with hot spots.

2011], propagation influences of turbulence and internal gravity waves [e.g., *Gibson et al.*, 2010; *Kulichkov et al.*, 2010], nonlinear propagation algorithms [*Blanc-Benon et al.*, 2002; *Kulichkov*, 2008], and approaches for temperature and wind structure inversions [e.g., *Garcés*, 2004; *Haney*, 2009]. Experience from seismology has shown that rigorous testing of these hypotheses and models requires dense networks of sensors and repeating sources of infrasound.

[4] The USArray is a dense network of approximately 400 broadband seismometers spanning the western U.S. during 2007–08 with an average station spacing of 70 km [*Busby et al.*, 2006]. Although seismometers directly measure ground motion, it has been long known that they also indirectly measure other phenomena that affect ground motion [e.g., *Kanamori et al.*, 1991; *Kappus and Vernon*, 1991; *Qamar*, 1995; *Ishihara et al.*, 2003; *Edwards and Hildebrand*, 2004; *Langston*, 2004; *Cochran and Shearer*, 2006; *Arrowsmith et al.*, 2007]. Specifically, atmospheric infrasonic wavefronts graze the Earth's surface, creating acoustic-to-seismic coupled signals with move out velocities (also known as "celerities") between ~180 and ~330 m/s depending on the turning height of the ducted ray. Pressure disturbances can also impart signals in seismometer data that are unrelated to ground displacement. Distinguishing between such mechanisms requires collocated acoustic and seismic sensors. The results from this study are independent of the mechanism(s) involved in the creation of the seismometer signals. For descriptive purposes we refer to any signals recorded by seismometers that have such group velocities as "acoustic-to-seismic coupled" signals.

[5] Recently acoustic-to-seismic coupled USArray recordings of a bolide explosion in northeast Oregon have showed that the relatively dense spatial sampling of the infrasonic wavefield illuminates the source location [*Walker et al.*, 2010] as well as the nature of infrasonic propagation [*Hedlin et al.*, 2010; *de Groot-Hedlin et al.*, 2011] in unprecedented resolution. The success of the Oregon bolide studies suggest that the sampling of infrasonic wavefronts every 70 km over several thousand kilometers distance for multiple events may provide an unparalleled data set for testing infrasonic propagation hypotheses and atmospheric velocity models, perhaps even defining a new construct for basic infrasonic research.

[6] In this study we use the method presented by *Walker et al.* [2010] and reverse time migrate acoustic-to-seismic coupled signals recorded by the 2007–08 USArray to detect and locate in two-dimensional space and time sources of atmospheric infrasound in the western U.S. This method is similar to that used by *Shearer* [1994] and *Ekström et al.* [2003] to locate previously undetected earthquakes primarily using surface waves. We present two catalogs totaling 901 infrasonic events. We show that the spatial distribution of events defines several repeating sources of infrasound, or "infrasonic hot spots" in the western U.S. We present two examples of these events as well as event detection, location and time accuracy, and propagation statistics for both catalogs. Our results are significant in several ways. To our knowledge, this work represents the first large-scale infrasonic source detection and location study using a relatively dense network of single-sensor stations that are able to fill in the gaps between globally spaced infrasound arrays, providing spatial detection and propagation pattern delineations of stratospherically ducted infrasound in unprecedented resolution. The success of the methods presented here suggests that they may be used with regional seismic networks near nuclear test monitoring infrasonic arrays to reduce the false alarm rate by locating nearby repeating sources of infrasound. Our results also provide a basic framework with which one may analyze and interpret infrasonic waveforms recorded by the soon-to-be-deployed broadband acoustic component of the USArray, or "acoustic USArray" [e.g., *Vernon et al.*, 2010].

2. Study Region and Data

[7] The Earthscope USArray comprises about 400 broadband, three-component seismic stations with an average interstation spacing of ~70 km. Most of the stations in this array are continuously being redeployed station-by-station to "roll" across the continental United States in ~9 years. The average stationary time for each station is 24 months. The USArray in 2007–08 spanned about 2 million square kilometers (Figure 1). The network fully spanned all the western U.S. coastal states during 2007. Most of the seismometers west of the −118° meridian moved farther east in the spring of 2008. There are two important aspects of USArray site selection that benefits our study. The first is that the 70-km station spacing creates a nearly uniform Cartesian grid of stations. The second is the criterion that all sites have relatively similar site conditions; the sites are all in soil rather than on various types of media, which helps reduce the variations in acoustic-to-seismic coupling across the USArray.

[8] The 2007–08 USArray encompassed several sources of known or possible infrasonic activity. One possible source is surface-mine and quarry blasting [e.g., *Sorrells et al.*, 1997; *Hagerty et al.*, 2002; *Stump et al.*, 2002; *McKenna et al.*, 2007; *Arrowsmith et al.*, 2008]. The USGS seismically

locates mine blasts (http://earthquake.usgs.gov/earthquakes/eqarchives/mineblast/). The University of Washington seismic network is also used to identify quarry blasts in Oregon and Washington. Several tens of mining events are shown in Figure 1 with a local Richter magnitude (M_L) between 2 and 3. The USGS has identified the activities that are associated with most of the blasts in their archive. Although no information is provided for the northern Nevada events, the blasts in eastern Arizona, western New Mexico, central and western Utah, Colorado, and Wyoming were likely due to surface copper and coal mining [*Richins*, 1979; *Arabasz et al.*, 1997]. The largest and most energetic surface mining activity (M_L typically 2.8 to 3.6) is in the Powder River basin in northeast Wyoming [*Arrowsmith et al.*, 2008], but this site is to the east and outside of the 2007–08 USArray making detection of any associated infrasonic signals more challenging, especially during the winter when stratospheric winds blow toward the east.

[9] In addition to infrasound generation from mine and quarry blasts, military aircraft training areas, bombing ranges, missile and rocket launch sites, and ordinance disposal sites can also generate infrasound (red stars in Figure 1). Infrasonic energy recorded from some of these sites has been previously studied. For example, the Hawthorne Army Depot is an ordinance disposal site near the western Nevada border. *Negraru et al.* [2010] used the routine explosions at that site to investigate the time-varying nature of the penetration of infrasound into the "zone of silence," which is a geometric shadow zone out to about 200 km range predicted by ray tracing of stratospherically refracted infrasound that initially propagates upward from a surface event [*Gutenberg*, 1939].

[10] Another location of known activity is the Utah Test and Training Range (UTTR), located just west of the Great Salt Lake in Utah. UTTR is the largest overland contiguous block of supersonic-authorized restricted airspace in the western U.S. and partners on military training exercises with Dugway Proving Ground (DPG), located 100 km to the south. In addition, UTTR is frequently used to dispose of explosive ordinance. A study of acoustic-to-seismic coupled signals from the UTTR events with the USArray and the High Lava Plains IRIS PASSCAL seismic array shows that the G2S mesoscale models explained many of the arrivals (M. Hedlin, personal communication, 2011).

[11] Southern California is known to be a location of routine infrasonic activity. *Cochran and Shearer* [2006] applied a cross-correlation technique to envelope functions recorded by the Southern California Seismic Network. They located infrasonic events off the coast of southern California, presumably associated with military training activities.

[12] There are a number of other sites in the western U.S. that may give rise to infrasound. To our knowledge, infrasound emissions from such sites have not yet been documented. Southwest Idaho is home to the Mountain Home Air Force Base. This base uses two bombing ranges for training purposes: Saylor Creek and Juniper Butte ranges. In addition, Edwards Air Force Base, China Lake Naval Weapons Station, and Fort Irwin Military Reservation in the northeast Mojave Desert comprise a special use airspace that includes bombing ranges and supersonic corridors.

[13] There was a permanent infrasound array called NVIAR designed to detect infrasound in the 0.05 to 5 Hz range near Mina, Nevada during 2007–08. Operated by Southern Methodist University, this array comprises four low-frequency microphones attached to microporous hoses for wind noise reduction [e.g., *Walker and Hedlin*, 2010].

3. Method

[14] We use the method of reverse time migration (RTM) to detect and locate sources of infrasound. RTM originates from the exploration seismology community [e.g., *Claerbout*, 1971; *Stolt*, 1978; *McMechan*, 1983]. With the advancement of computers and larger sensor networks, this imaging method is now being applied to many academic, engineering, and medical problems. Each problem has a specific focus and context, leading to a variety of different names including "back projection," "source scanning," "time reversal," and "stacking."

[15] RTM is used to illuminate sources of energy that propagate to many receivers. These sources may be secondary sources such as seismic reflectors or scatterers, or primary sources such as earthquakes or explosions. One typically assumes a propagation velocity model and predicts the travel times from all possible source locations to the receivers. With these predicted travel times, RTM "back projects" the energy in time in all possible spatial directions by summing observed energy at each station that aligns in time with the predicted travel times for each possible source location. If the energy is aligning in phase, then the energy will constructively interfere upon summation (stacking). Conversely, energy that is out-of-phase will destructively interfere. Ignoring variations in amplitudes and source-receiver geometric factors, the signal-to-noise ratio in dB for the "stacks" for wavelengths with coherence distances less than the station spacing interval is predicted by $10 \log_{10}(N)$, where N is the number of receivers. Longer wavelengths will have a reduced signal-to-noise ratio (SNR) gain. Images are generated by taking cross-sections through the multidimensional stacks. The final problem of identifying sources is reduced to finding significant peaks in these images.

[16] The method used in this paper is a modified version of that described quantitatively by *Walker et al.* [2010]. We only briefly discuss the technique here. The vertical broadband seismic records are band pass filtered between 1 and 5 Hz. Because the RTM method requires phase coherence between adjacent sensors (and infrasonic signals have coherence lengths of only ~1–2 km), we calculate the envelope functions of these filtered data. The envelopes are then decimated to a sampling rate of 10 mHz to regularize the envelope durations. This often results in just a handful of time samples representing several acoustic-to-seismic coupled arrivals at each station. Automatic gain control with a time window 1000 s long is applied to regularize the running maximum amplitude of the decimated envelopes to disable a handful of stations with high noise levels from masking the detection of an event. These steps define the preprocessed waveforms.

[17] RTM requires a velocity model to calculate the predicted source-receiver travel times. However, for problems of primary source imaging, one does not require a priori knowledge of the correct velocity model. We assume a range of trial, isotropic, linear move out velocities (also called "celerities") for the seismic-to-acoustic coupled signals of 280 to 350 m/s, with an interval of 10 m/s. For each of these

celerities, which are tuned to detect stratospheric and tropospheric arrivals, we perform RTM on 24 h of preprocessed waveforms using an X/Y/T source parameter grid. The time sampling interval was 100 s. For 280 and 350 m/s celerities, the spatial distance a signal traverses ranges from 28 to 35 km. The space grid had an X and Y sampling interval of 20 and 24 km, respectively. For each day, the grid was 2,000 km (E–W) by 2,400 km (N–S) centered on the mean latitude and longitude of the stations that were used. Source altitude is ignored (assumed to be 0) because there is no altitude resolving power at ranges greater than ~100 km.

[18] Two record sections of signals from roughly spatially collocated events near the southwest corner of Idaho in the summer and winter demonstrate the optimum alignment of preprocessed energy determined by RTM (Figure 2). To reduce the number of pure-noise waveforms for plotting purposes, we selected only stations to the west and southeast of the epicenters, respectively. The 1 to 5 Hz bandpass filtered waveforms contain relatively high-frequency signals that generally do not align well. However, the corresponding decimated envelope functions align well, showing that our assumption of a homogeneous, isotropic velocity model is adequate to first order for source location purposes.

[19] The RTM process results in a stack function $S(x, y, t, v)$, where x, y, t, and v are longitude, latitude, time, and celerity, respectively. Because of the application of the automatic gain control to the preprocessed waveforms, peaks in S indicate coherence of envelope energy rather than the sum of envelope energy along an infrasonic travel-time curve. For detecting sources in S, we calculate a detector function $Q(t)$ that is the maximum value of S looking in the x, y, and v directions. A six-hour, high-pass filter is subsequently applied to Q. The signal-to-noise ratio (SNR) of each peak in Q is calculated by converting the peak amplitude to dB with respect to the daily median value. Peaks with values greater than 15 dB are generally considered significant and may indicate possible events.

[20] An automated approach would be ideal for detecting events in $S(x, y, t, v)$. However, to gain insight into the problems that might occur with an automated approach, we manually inspected and picked maxima in Q that were classified as detections. A picking interface was developed for this process, which we refer to as Phase I (Figure 3). The analyst initially looks for maxima in Q above ~15 dB (Figure 3a). A maximum is then picked, which defines x_p, y_p, t_p, and v_p. The click updates both a map with a cross-section through $S(x, y, t_p, v_p)$ (Figure 3b) and a record section of envelope functions versus range from (x_p, y_p) (Figure 3c). The receivers that were used in the image can be shown on the map. The analyst can isolate only stations in certain source-to-receiver azimuth ranges and distances to investigate what stations contribute the most to the peaks in Q. The analyst also inspects large teleseismic, regional, and local earthquake times and positions to investigate correlations or complexities. Visual discrimination between seismic and acoustic-to-seismic signals is relatively easy due to the much faster seismic apparent velocities. Such seismic signals show as nearly horizontal lines in the record section. If the picked acoustic event is considered significant, the analyst assigns the event a grade of A, B, or C, with "C" representing a probable event with a relatively low SNR. Typical "A" events are clearly detected past 500 km range and have signal-to-noise ratios above 25 dB. Typical "C" events have a range out to 200 km and SNR between 10 and 20 dB.

[21] Although it is known that the human eye can detect lineations in noisy data fairly well, we recognize that this adds an element of subjectivity. To quantify the goodness-of-fit between the aligned energy and our optimum source parameters, "Phase II" of our method is a bootstrap analysis of the A and B events to estimate uncertainties [*Efron and Tibshirani*, 1993]. A significant peak in S defines the ith event. For each ith event we resample with replacement $B = 100$ times the full set of stations used in the RTM process that defined S. For each resampling, centered on the pick location and time, we modify the source location grid to span 600 × 660 km yielding an X/Y intervals of 6.0 and 6.6 km, respectively. We also reduce the length of the time grid to 30 min and broaden the celerity range from 250 to 350 m/s. This generates a new $S^B{}_i(x, y, t, v)$ and $Q^B{}_i(t)$. The maximum value over time in $Q^B{}_i(t)$ is found, and the associated optimum parameters for this bootstrap-resampled event location are saved. We characterize uncertainties in source location with the smallest geographic uncertainty ellipse that encloses 67% of the 100 bootstrap locations. To find these ellipses we perform a grid search over the parameters that control the location, size, and shape of the ellipse to minimize an objective function defined by

$$M = a|P_e - 0.67| + b(A_e/A_g) \quad (1)$$

where P_e is the proportion of bootstrap locations inside the trial ellipse, A_e and A_g are the areas of the ellipse and Phase II grid, and a and b are weights chosen to be 1 and 3 based on numerical experiments, respectively. In order to obtain uncertainties in source time and move out velocity, we calculate the means of the bootstrap results and the probability distribution function, from which the 67% confidence interval is obtained.

[22] The uncertainty analysis may fail to constrain the optimum Phase I parameters. This condition is detected if any one of the following quality-control criteria are true: (1) the best fit ellipse does not enclose the Phase I location, (2) the best fit ellipse does not enclose the mean of the bootstrap locations due to a significant number of outliers, (3) the best fit ellipse encloses less than 60% of the bootstrap locations, or (4) more than 33.3% of all the bootstrap optimum parameters occurred along a grid boundary. The picked events that pass these quality control tests are considered to be of high quality. All other picked events are considered as events with unconstrained uncertainties that could be constrained by further analysis.

4. Results

[23] The method was applied to the 2007–08 USArray data and detected a total of 901 events. These 901 events define the Western U.S. Infrasonic Catalog version 1 (WUSIC-1). Specifically, 227 are classified as "high-quality" (WUSIC-1A; Table S1 in the auxiliary material), and the remaining 674 events have unconstrained uncertainties (WUSIC-1B; Table S2 in the auxiliary material).[1] The

[1] Auxiliary materials are available in the HTML. doi:10.1029/2011JB008579.

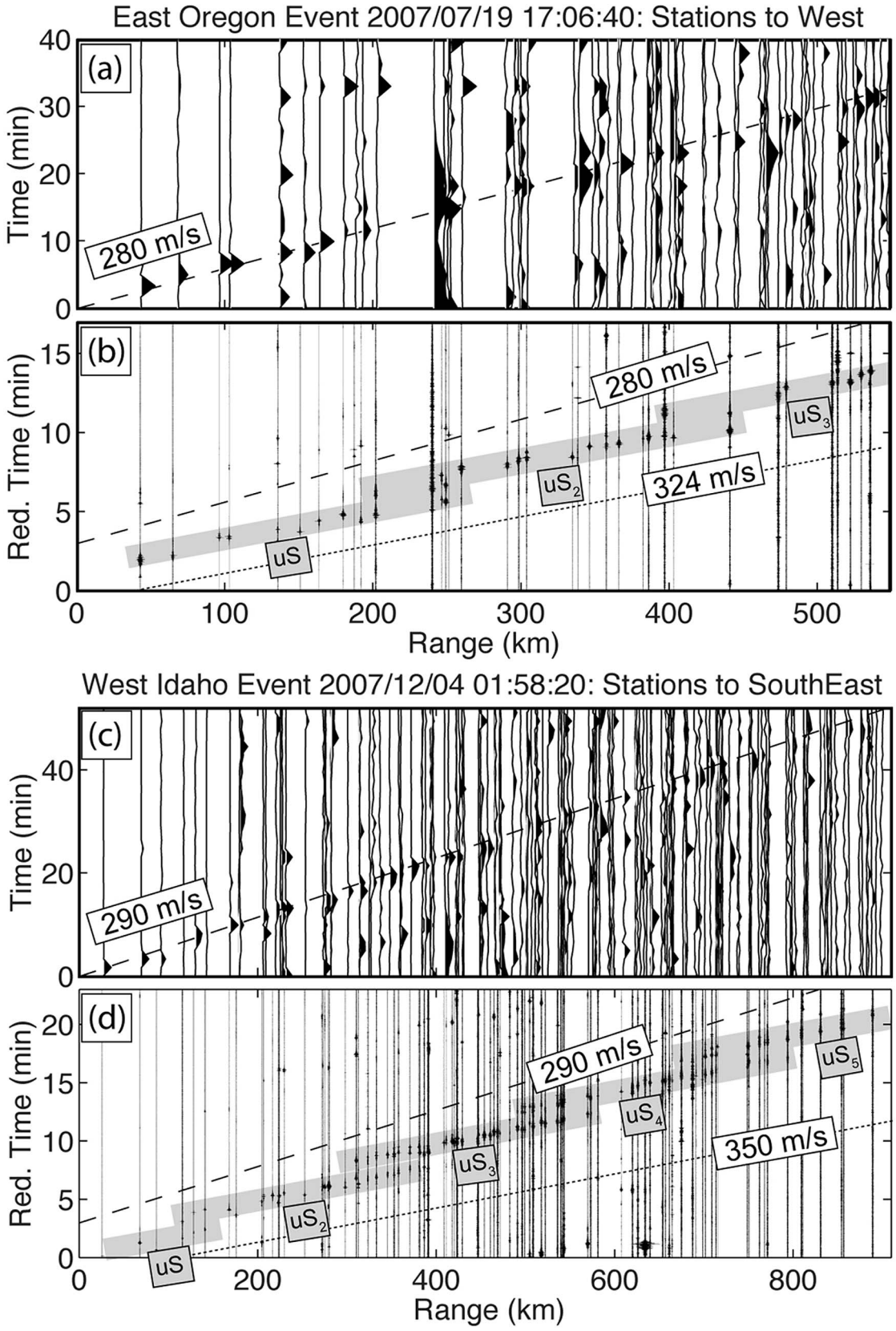
East Oregon Event 2007/07/19 17:06:40: Stations to West
(a)
280 m/s
Time (min)
(b)
280 m/s
uS3
uS2
324 m/s
uS
Red. Time (min)
Range (km)
West Idaho Event 2007/12/04 01:58:20: Stations to SouthEast
(c)
290 m/s
Time (min)
(d)
290 m/s
uS5
uS4
uS3
350 m/s
uS2
uS
Red. Time (min)
Range (km)

Figure 2

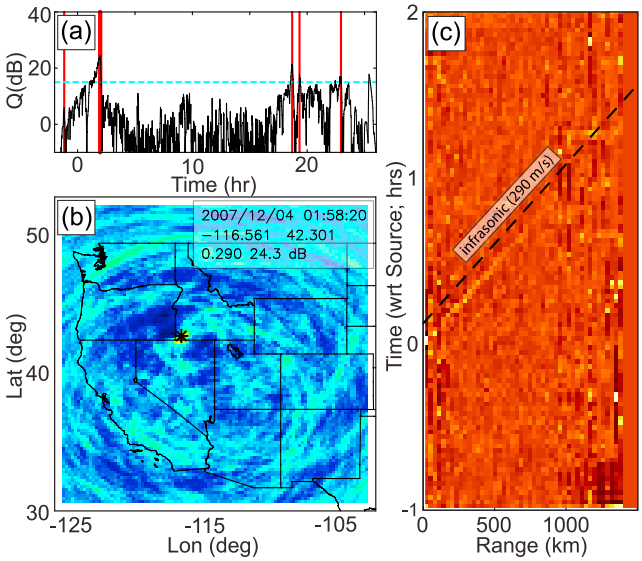

Figure 3. Example of picking interface for an event in southwest Idaho. This event is the wintertime event shown in Figure 2, which received an "A" rating.

following subsections describe the spatiotemporal event distributions and statistics, quantify the source location accuracies, and illuminate propagation patterns.

4.1. Spatial Distribution of Events

[24] The locations of most events generally cluster in four areas: south Nevada, central Nevada, northwest Utah, and southwest Idaho (Figure 4). Although we prefer to show the spatial distribution of both the constrained and unconstrained events, the hot spots are smaller in size if the unconstrained events are excluded.

[25] There is no significant correlation between the shallow mining and quarry blasts (Figure 1) and the hot spots. In addition, none of the shallow mine and quarry blasts listed in the USGS or University of Washington catalogs (Figure 1) were detected by our method. This could be explained if most of the energy in these events is being used to fragment solid earth instead of compress air.

[26] There is a good correlation between the potentially infrasonically active military areas and the hot spots (Figure 4). The hot spot in southwest Idaho may be associated with surface explosions or supersonic aircraft during training activities out of Mountain Home AFB. Furthermore, there is no mining activity in southwest Idaho (B. Phillips, Idaho Geological Survey, personal communication, 2011).

[27] In northwestern Utah is the UTTR ordinance disposal site, where Trident rocket motors are detonated on the surface. The UTTR events in 2007 range in net explosive weight up to ~17,500 kg (Table S3 in the auxiliary material) (R. Berlacu, personal communication, 2010). A significant number of events are detected there, some of which are not reported. To the south of UTTR is Dugway Proving Grounds, where supersonic flights are expected to occur routinely and a large number of events are also detected.

[28] In central western Nevada are the Bravo 16, 17, 19, and 20 bombing ranges, which are associated with Fallon Naval Air Station. The central Nevada hot spot, which occurs just to the east of these ranges, is likely due to surface detonations or supersonic aircraft. Signals from this hot spot are consistent with signal back azimuths observed at nearby infrasonic array NVIAR.

[29] Directly south of the Bravo bombing ranges, adjacent to NVIAR, is the Hawthorne ordinance disposal site where surface blasts occur routinely and a large number of events are detected. The envelopes of these signals are a bit broader than envelopes from signals from other hot spots because the Hawthorne signals usually consist of several impulsive events, each separated by several tens of seconds [*Negraru et al.*, 2010].

[30] It is public knowledge that the Nellis Air Force Range is a possible infrasonic source due to supersonic aircraft activity. Furthermore, the adjacent Nevada Test Site routinely conducts subcritical explosions for testing purposes. This broad area indeed correlates with the location of the most infrasonically productive hot spot in the western U.S.

[31] Last, the China Lake bombing range and Edwards Air Force Base (often considered the home of supersonic test flights) are also associated with detected events. Some events were also detected off the coast of San Diego (in a known military testing area) and near Vandenberg Air Force base. The possible infrasonic sources along the New Mexico and Arizona edge of the USArray do not correlate with hot spots. This may reflect a detection issue (perhaps associated with relatively poor source-receiver geometry) or a lack of activity at those sites.

4.2. Temporal Distribution of Events

[32] If our approach works well to detect and locate routine infrasonic activity in the western U.S., and assuming the USArray is stationary, we should expect to see similar rates-of-occurrence during the day, week, and year for both 2007 and 2008. Indeed, this is what is observed in the analysis of all A-C events (Figure 5). The local time-of-day histograms have a peak from 10 A.M. until noon and a noticeable dip between 1 and 2 P.M. The day-of-week histograms are peaked on Wednesday and Thursday, with the fewest number of events on Sunday. If this is purely a source effect, this distribution suggests that most signals are related to human work-related activities that do not stop at 5 P.M., but continue until about 10 P.M. with a lunchtime reduction in activity.

[33] Although the day and week rate-of-occurrences are similar for both years, there are different year rate-of-occurrences for both 2007 and 2008 (Figure 6a). On average, there are about 40 events per month during both years, except for a general gap in detections during the time

Figure 2. Record sections of a summertime and wintertime event near the southwest Idaho corner. Shown are (a, c) the envelope functions that have been resampled at 10 mHz (without automatic gain control) and (b, d) the original 1 to 5 Hz USArray, vertical-component seismic data sampled at 40 Hz for stations to the west of the summertime event and to the southeast of the wintertime event for signal-to-noise ratios greater than 0 dB. Dashed lines indicate the optimum celerities (280 m/s and 290 m/s, respectively). Gray rectangles in Figure 2b illuminate the different arrivals, which have higher move out velocities than the optimum celerity obtained by the RTM analysis.

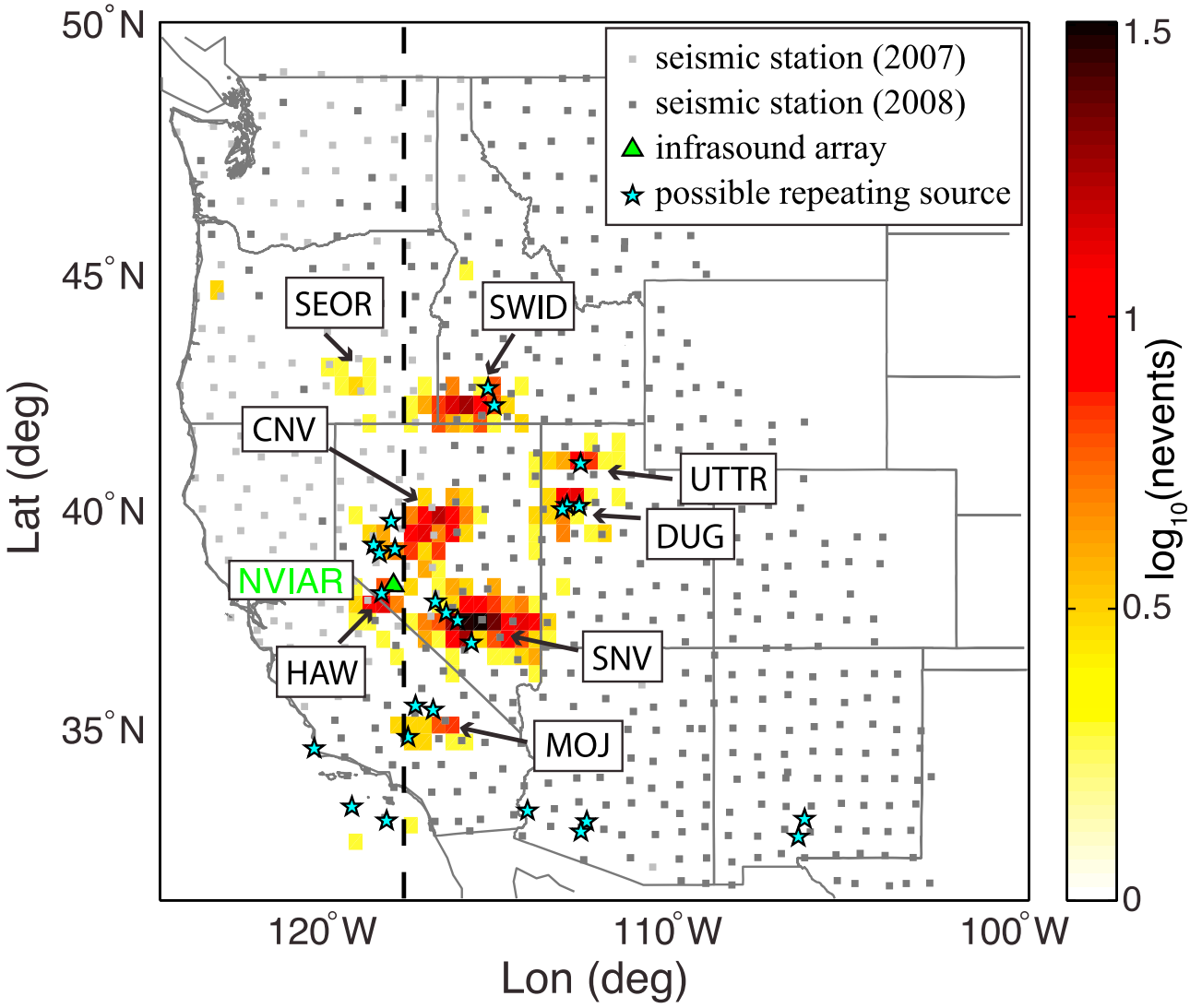

Figure 4. Two-dimensional histogram showing imaged source locations for A-C events in 2007–08 defining "hot spots" of activity (labels). Stars indicate military areas of potential infrasonic emissions that spatially correlate with hot spots.

period 05/2008 - 09/2008. If the gap were due to a source or seasonal propagation effect, one would expect the same summertime gap during 2007. We ascribe the 2008 summertime gap to the 09/2007 – 05/2008 movement of stations west of the Nevada hot spots (meridian 118°W; Figure 4) to the east such that by the time the westward stratospheric winds resume in the summer of 2008, there are not enough stations west of the hot spots for event detection (Figure 6b).

4.3. Source Location and Time Accuracy

[34] The source location and time accuracy of our approach depends in part on the density of the station network and RTM grid. To assess the accuracy of the results in the WUSIC-1A catalog, we compare estimated source parameters and uncertainties to the known parameters of several events detonated at the UTTR test facility in western Utah (Figure 7). We define "spatial accuracy" to be half of the average size of the uncertainty ellipse long axes, if the ellipses typically enclose the true known event location and

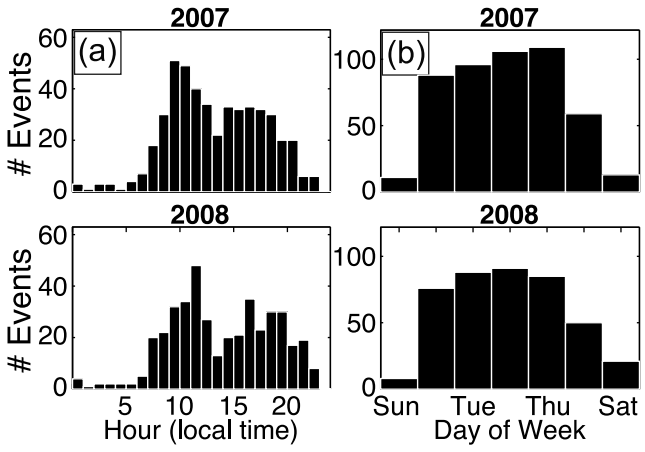

Figure 5. Histograms of source times for all located events. The rate-of-occurrence versus (a) day-hour and (b) weekday shows that most detected events occurred during the work-week daytime.

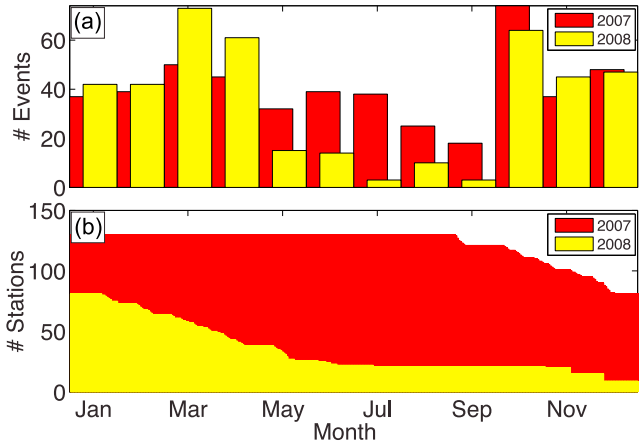

Figure 6. Analysis of detection gap during the summer of 2008. (a) Yearly histograms of all located source dates. (b) Corresponding number of USArray stations to the west of −118 deg longitude. The histograms correlate from month to month, except during the summers. The drop in detections during the summer of 2008, when westward propagation is favored due to seasonal stratospheric winds, is explained by the 9/2007 to 5/2008 redeployment of stations from west of central Nevada to east of Nevada. Detection of signals to the east of Nevada begins occurring due to the reversal of the stratospheric winds in October 2008 (specifically around 10/06).

time. There are 12 known events that occurred at the UTTR site in 2007 (Table S3 in the auxiliary material) (R. Bercalu, personal communication, 2010). Of these events, nine were detected by our technique. Four events did not pass the phase 2 quality control thresholds (WUSIC-1B catalog). The remaining five events have 67% confidence ellipses that overlap the known event location, with semi-major axes ranging in length from 86 to 108 km (Figure 7a), yielding a spatial accuracy of 50 km for the UTTR events.

[35] The source time determined by our approach does not agree perfectly with the known source time (Figure 7b). The residual time (observed minus known) is shown for the picked times (from Phase I) and the bootstrap means (from Phase II). One should expect an accuracy of ±50 s since the RTM and bootstrap time sampling interval is 100 s. We find that the optimum source times are about one sample early, and the 67% confidence interval spans the known source time for 50% of the events. Given this bias, the temporal accuracy of the UTTR events is ± 120 s. While this inaccuracy is not great relative to the RTM and bootstrap sampling interval, it warrants further understanding and is discussed later.

[36] It is useful to compare the shape and size of the ellipses for the UTTR hot spot to those of the other ellipses from unknown events in other regions (Figure 8). Histograms of the lengths of the semi-major and semi-minor axes as well as the azimuths of the semi-major axes show that the UTTR ellipses are generally representative of ellipses from other hot spots. It should be noted that the UTTR ellipses in Figure 8 include three additional high-quality events that were previously unreported. Considering all the events together, the distributions are roughly normally distributed with an average semi-major axis length of 92 km, leading to an average spatial accuracy estimate of about 50 km for all the events in the WUSIC-1A catalog. The shortest and largest 67% confidence ellipses are 11 and 204 km, respectively. The average semi-major axis azimuth is 77°, with a standard deviation that includes the east-west plane. As will be discussed later, the consistency of the ellipse orientation for hot spots throughout the 2007–08 USArray suggests this is not a product of poor source-receiver geometry, but instead a result of anisotropic infrasonic ducting due to east-west stratospheric winds.

4.4. Propagation Patterns

[37] The uncertainty in the source location and time for atmospheric point sources detected with our approach will be exceptionally small if resulting signals are detected by stations at all azimuths and ranges. Several spatial analyses of the stations with significant signals that contributed to the detected events showed that the signals are often ducted in one predominant direction. For example, two events from near the corner of southwest Idaho during summer and winter months show that stations with significant signal-to-noise ratios (above 0 dB–a different definition than used for the detector function) are generally to the west and southeast of the epicenters, respectively (Figures 2 and 9). There are several lines of evidence that suggest that these are stratospherically ducted arrivals. The anisotropic ducting directions correlate with the general expected directions of the seasonal stratospheric winds [*Le Pichon et al.*, 2009]. Furthermore, the optimum celerities are 280 and 290 m/s, which suggest the ducted rays turned in the stratosphere. Finally, three-dimensional ray tracing was performed on the summertime event using a high-resolution "mesoscale G2S-NRL" atmospheric velocity model [*Drob*, 2010]. The predicted arrivals to the west of the epicenter are stratospherically

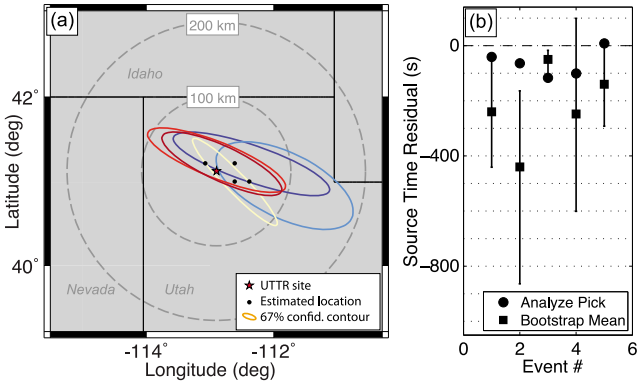

Figure 7. Location accuracy analysis. (a) Map view of USArray-located rocket motor detonations and 67% confidence ellipses for the five reported blasts in 2007 that are in the WUSIC-1A. The ellipse color map indicates the date of the event ranging from early June (blue) to late August (red). UTTR site is shown as a red star. (b) Source time residuals (observed-actual) showing that half the source times are within the 67% confidence intervals indicating a bias in the estimation of source time. Note that the source time sampling interval for the RTM and bootstrap uncertainty analysis is 100 s.

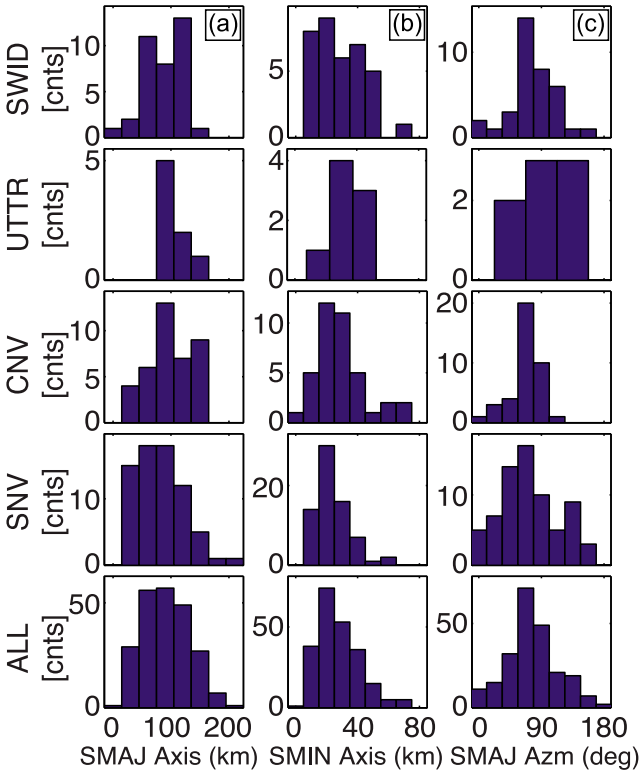

Figure 8. Histograms of the shape parameters for the 67% confidence ellipses of events in clusters SWID, UTTR, CNV, and SNV, as well as for all events in WUSIC-1A. Shown are the distributions for the (a) semi-major axes lengths, (b) semi-minor axes lengths, and (c) semi-major axes azimuths. In general, the distributions are well behaved; the predominant ellipse has a 92 km length, 27 km width, and 77° azimuth.

ducted and agree fairly well with the observations, suggesting that the arrivals are uS, uS_2, uS_3, uS_4, and uS_5 using the arrival branch nomenclature introduced by *Hedlin et al.* [2010] (Figure 2).

[38] The celerities for the WUSIC-1A events are normally distributed with an average value of 295 m/s (Figure 10). This celerity and the well-behaved distribution also suggest that the predominant infrasonic arrivals that have been detected are stratospherically ducted. Expanding this into a 2-D histogram in time shows a sinusoidal variation with a 12-month periodicity. To represent this variation with a waveform, we calculate the median value in 45-day bins when enough data are available. The standard deviations are provided by the bootstrap method.

[39] The observed seasonal variation indicates higher celerities during the summertime. Because Nevada contains the most events, we plot the vertically averaged temperature provided by G2S atmospheric specifications for 0 to 15 km altitude and 0 to 50 km altitude [*Drob*, 2010]. From these daily temperature averages, we also calculate the median value in 45-day bins. Assuming the G2S temperature profiles are accurate up to 50 km, if the event raypaths were predominantly within a ground-to-stratosphere duct, one would expect a better correlation with the 0 to 50 km temperature average. If the raypaths were predominantly within a tropospheric duct, one would expect a better correlation with a 0 to 15 km temperature average. The optimum correlation is with the 0 to 15 km temperature average and is discussed in more detail later.

5. Discussion

5.1. Spatiotemporal Distribution and Origin of Infrasonic Events

[40] The temporal distribution of the 901 located events suggests that the predominant origin is human activity

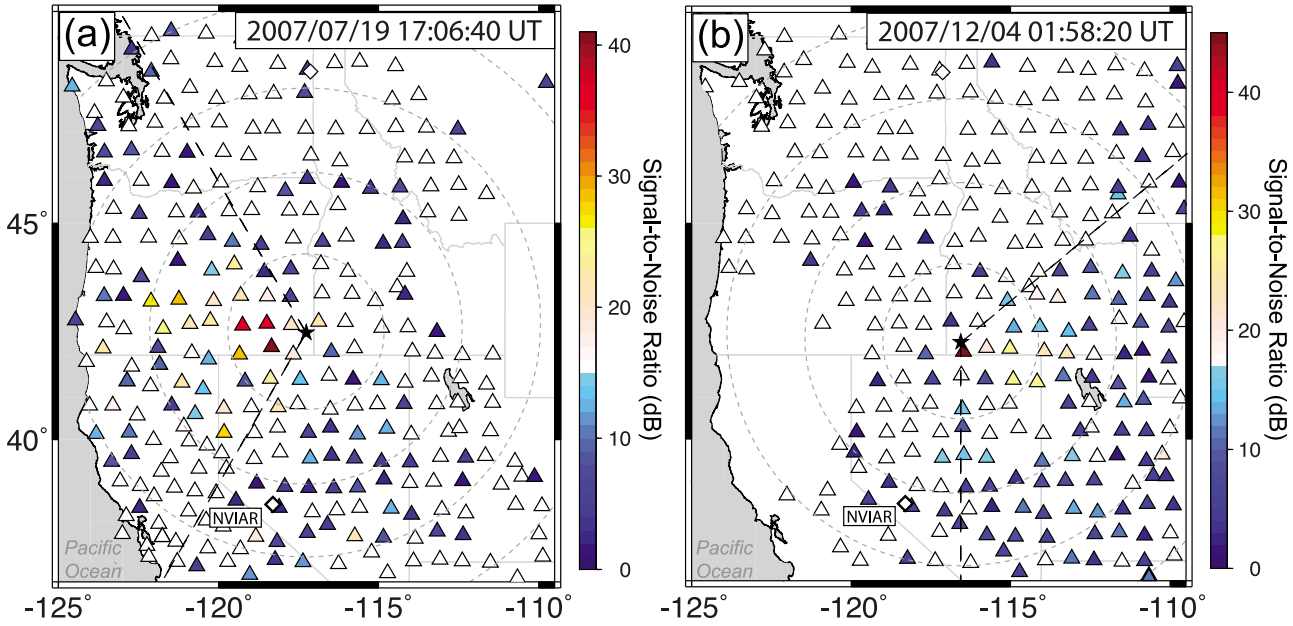

Figure 9. An example of (a) eastward and (b) westward ducting demonstrated by map views of stations color-coded by signal-to-noise ratio. The dashed lines indicate the azimuth range used to select waveforms for plotting in Figure 2. The concentric circles expand out in 200 km increments.

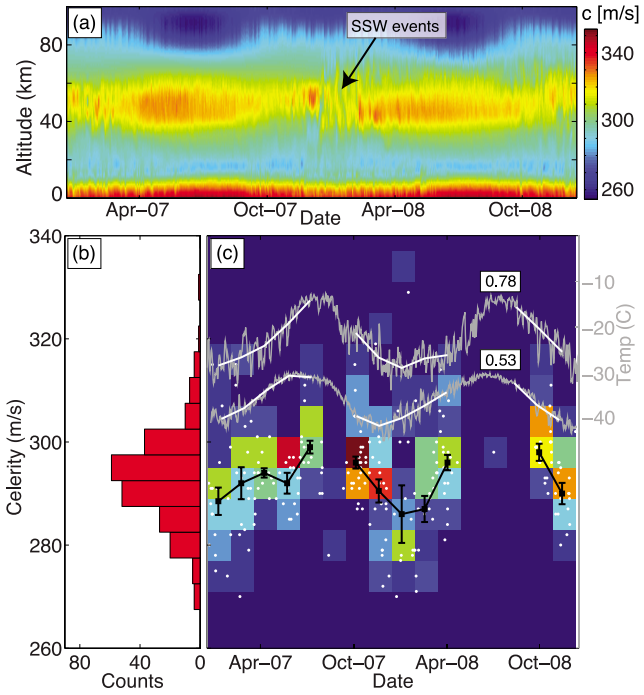

Figure 10. Inspection of trends in the detected events optimum average celerities. (a) The daily static sound speed profile based on G2S atmospheric specification of temperature at 12:00 UT versus time and altitude. The sudden stratospheric warming (SSW) events of January and February 2008 are clearly represented [*Wang and Alexander*, 2009]. (b) A histogram of the observed optimum celerities. The mean bootstrap celerities are plotted, which have a finer granularity than the Phase I celerities. (c) Expansion of the histogram along the time axis, where color indicates relative rate of occurrence. The black overlying curve and uncertainties are the median values in 45-day bins. The gray, thinner time series indicate daily temperature averaged over an altitude range, with the thicker overlying curves being the median for 45-day bins. The correlation coefficient between the temperature curves and celerity curve are indicated for the 0 to 50 km average (0.53) and 0 to 15 km average (0.78).

associated with the workweek; if the events were due to a natural process, one would not expect to find a significant lack of events during the weekend (Figure 5). Furthermore, the spatial distribution of events correlates with areas of publicly known U.S. military testing and training activities (Figure 4). Correlation of locations of well-detected events with known explosions on the surface at UTTR and Hawthorne indicates that our method is detecting and locating surface explosions fairly accurately and deriving meaningful confidence regions (Figure 7). The source uncertainty statistics of the UTTR events are representative of the other located events from unknown sources (Figure 8). For many of these UTTR events, the picking analyst observed in the record section not only the infrasonic wavefront, but also the seismic wavefront (1 to 5 Hz P waves and S waves).

[41] Much of the hot spot activity may be related to supersonic aircraft, which do not produce arrivals traveling at seismic apparent velocities. In the absence of anisotropic ducting that selects a preferred propagation direction, a sonic boom due to a brief moment of supersonic flight would be seen in only two quadrants, and at greater ranges, would appear to come from a point source. With anisotropic ducting encouraged by stratospheric winds, only one of the two propagation directions would return energy to the Earth's surface. Extended durations of supersonic flight would give rise to infrasonic line or curve sources that would not be located accurately with the above approach. Such cases would give rise to time-extended and poorly defined peaks in the detector function Q and prominent but non-intersecting circles of energy in map view (Figure 3). Although this was occasionally observed by the picking analyst, especially in the Mojave desert area, most of the signals were coherent and well located.

[42] No infrasonic arrivals from shallow mines or quarry blasts were detected by our approach (Figures 1 and 4). Mining explosions are engineered to fragment solid earth rather than generate infrasonic energy. Furthermore, quarry blasts would also have less energy propagation horizontally away from the site if the detonation point was in a local topographic depression. However, blasts from the Powder River Basin have been detected infrasonically over hundreds to thousands of kilometers by an infrasonic array in southern Canada (IS10) [*Bahavar et al.*, 2007]. As the USArray moves east and encompasses Powder River Basin, the most active area of large coal mine blasting, future investigations will determine the extent to which seismic sensors can detect shallow mine and quarry blast infrasonic signals.

5.2. Source Parameter Accuracy

[43] The UTTR source location confidence ellipses generally span the true location and are also oriented east-west, with an average length of 94 km. The confidence ellipses for all events are on average oriented east-west with a 92 km length and 27 km width. The average accuracy for all the events in the WUSIC-1A catalog is therefore about 50 km. From inspection of the 1 to 5 Hz waveforms in Figure 2, it is clear that the energy does not align perfectly. This "residual" is likely due to three effects: (1) wind-induced velocity anisotropy, (2) divergence from a point-source model, such as might be expected for sources due to supersonic aircraft, and (3) 3-D velocity heterogeneity. The 901 event locations estimated here should be treated as a first pass upon which improvements can be made, for example, by inverting picked arrival times [e.g., *Ishihara et al.*, 2003; *Langston*, 2004; *Arrowsmith et al.*, 2007]. This approach was also used by *Walker et al.* [2010] to determine the source location and time of the 2008 February 19 bolide explosion in northeast Oregon, which was registered infrasonically by the USArray out to 800 km range. The resulting 95% uncertainty ellipse was 13 km long. This event is also in the catalog (#A156), which has a 51-km long 67% confidence ellipse that encloses the more precise solution obtained by analyzing only stations within 250 km of the source location.

[44] The known UTTR source times are on average 50–100 s later than we resolve (Figure 7). Although this is only a slight early bias with respect to the 100 s sampling interval, this observation merits discussion. An early bias for surface events can be explained by considering the optimum celerities observed in the arrivals from the two events near the southwest Idaho corner (Figure 2). The celerities for the summer and winter events align with the energy in the

decimated envelope functions. However, upon inspection of the original 1 to 5 Hz seismic data, one can see offsets between merging adjacent arrivals. The RTM approach effectively finds the best fitting line between the central points (in range) of the individual arrival branches. This causes the y-intercept to be earlier (in time) than the true source time and the best fit celerity to be slightly underestimated (lower than the celerity of the individual arrival branches). The X/Y source location accuracy is unaffected. It should be noted that the known source time for the 2008 Oregon bolide that exploded at 27 km altitude is 13:30:29 UT [*Walker et al.*, 2010]. The source time uncertainty determined using the above two-dimensional method (event #A156) spans the time interval from 13:30:00 to 13:31:40, which brackets the true source time.

5.3. Propagation Patterns and Statistics

[45] The classic "zone of silence" (ZoS) is a geometric shadow zone on the Earth's surface due to the time-varying and frequency-dependent propagation conditions of the atmosphere [*Gutenberg*, 1939]. Typical tropospheric, stratospheric, and thermospheric ducts will each have one or more ZoS. Sometimes infrasound is observed within a predicted ZoS [*de Groot-Hedlin et al.*, 2008; *McKenna et al.*, 2008; *Negraru et al.*, 2010]. A variety of hypotheses and approaches are developing to better explain such observations [*West et al.*, 1992; *Lingevitch et al.*, 1999; *Kallistratova*, 2002; *de Groot-Hedlin*, 2008; *Gibson et al.*, 2010; *Kulichkov et al.*, 2010]. The located events and associated acoustic-to-seismic coupled signals amount to roughly 100,000 waveforms that can be used to test these hypotheses and approaches [e.g., *Hedlin et al.*, 2010; *de Groot-Hedlin et al.*, 2011]. Just picking a single example, the observed signal-to-noise pattern for the summer and winter events (Figure 9) suggests that ducting to the west and east exists as expected for seasonal stratospheric winds, and that a ZoS does not exist for these events. Three-dimensional infrasonic ray tracing for the summer event using a G2S "mesoscale" model that includes Rapid Update Cycle (RUC) atmospheric specifications [*Drob*, 2010] generally confirms the lack of a ZoS in the western quadrant. Although an alignment of continuous infrasonic energy as a function of range was always observed during Phase I (Figure 3), it is premature to conclude that a ZoS is never observed in the western U.S. in the stratospheric downwind direction. Such a conclusion requires a quantitative analysis of the spatial arrival patterns of all 901 events and associated G2S atmospheric models.

[46] Although we find no seasonal trend in infrasonic event detection with the USArray, there is a clear trend in the celerities of the imaged events. The mean bootstrap celerities in the WUSIC-1A catalog (which have a finer granularity than the optimum Phase I celerities) have a seasonal variation that correlates at a level of 0.78 with a variation in both (1) the vertically averaged temperature from ground-to-space (G2S) models above central Nevada between 0 and 15 km altitude (troposphere; Figure 10) and (2) the daily average surface temperature obtained from several Nevada ground-based weather stations. Although the 78% correlation is remarkable and provides another validation that the detections are real, the good correlation is not unexpected. Atmospheric propagation is controlled by the effective sound speed, which is the sum of the static sound speed and wind speed in the propagation direction. Static sound speed $c(x, z)$ is proportional to square root of temperature (Figure 10a). Winds in the troposphere and stratosphere often vary by up to ± 40 m/s, which is only $\pm 15\%$ of c. Therefore, the dominant influence on celerity is atmospheric temperature along the raypath, and the amplitude of the 22% residual is generally consistent with variations in tropospheric wind jets. However, the mean observed celerity of 295 m/s (Figure 10b) is thought to be more consistent with rays turning at stratospheric heights. The 67% confidence region of the 0.78 correlation coefficient spans 0.62 to 0.87. When one performs the same analysis using an altitude range of 0 to 50 km to define the temperature waveform, the correlation reduces to 0.53 with a confidence region of 0.32 to 0.69 (Figure 10c). Comparing the two temperature curves yields a phase difference of $\sim$27 days, which is likely due to the effect of stratospheric anomalies like the Arctic Oscillation propagating down to the surface over the course of a few weeks [*Baldwin and Dunkerton*, 1999]. Optimally aligning the 0 to 50 km waveform with celerity provides a much improved correlation of 0.86. Therefore, the reduction in correlation with increasing altitude is due to this phase shift rather than stratospherically isolated events like sudden stratospheric warmings [*Craig and Hering*, 1959; *Evers and Siegmund*, 2009; *Wang and Alexander*, 2009; *Hedlin et al.*, 2010]. Regardless, the difference between the 0.78 and 0.53 correlations is not statistically significant. Although more data would be required in the gaps of the celerity curve to reduce the size of the confidence regions and better investigate the correlation, future studies may perhaps benefit more from using the catalogs presented in this study with automated phase identification and arrival time estimation programs to help validate and improve both the temperature and wind fields from which current atmospheric velocity models are derived.

5.4. Reducing False Alarm Rates for Systems Using IMS Infrasound Arrays

[47] Our results provide knowledge that may be useful in two ways to nuclear monitoring efforts at the CTBTO's International Data Center if the Comprehensive Nuclear-Test Ban Treaty enters into force. First, the hot spots identified in Figure 4 provide a basis for understanding future infrasonic events that might be located in the western U.S. by the global IMS infrasonic network.

[48] Second, the success of using our method on the USArray suggests that one could use the technique on permanent regional seismic networks around IMS infrasonic arrays to help locate new infrasonic hot spots as they arise around the arrays, which provides additional information that is helpful in distinguishing between regional background "noise" and signals of interest recorded by the arrays. For example, one can integrate the 2D histogram (Figure 4) along projected azimuths out to 500 km from NVIAR. This function can then be normalized by the total number of events included in the function to calculate a predicted array detection probability distribution function due to false alarms from regional events.

[49] Figure 11 shows the predicted NVIAR detection probability curve for the years 2007–08. For comparison, the back azimuth statistics of a year of high-amplitude NVIAR array detections are also shown. The detections were made

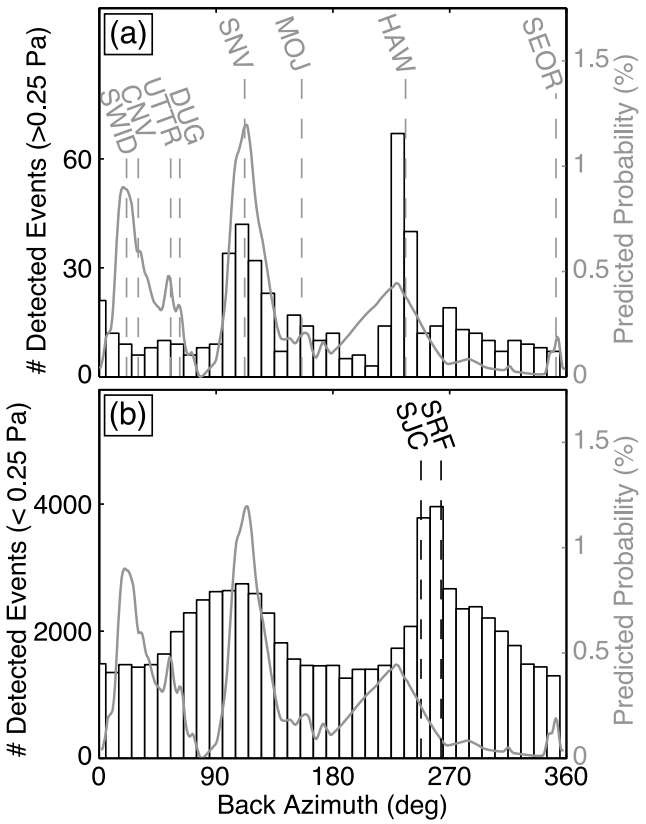

Figure 11. NVIAR infrasonic signals observed during 2007 compared with a predicted azimuthal probability distribution function using the 2D histogram statistics of the 2007–08 high-quality events (similar to Figure 4, but only for WUSIC-1A catalog). (a) Detections with amplitudes greater than 0.25 Pa correlate with the predictions for the SNV and HAW hot spots. (b) Detections with amplitudes less than 0.25 Pa exhibit a sinusoidal variation and do not correlate with the probability distribution function. The peak between 248° and 263° azimuth correlates with the San Francisco bay area.

using a time-progressive frequency domain beamforming approach similar to the PMCC method of *Cansi* [1995]. The predicted detection probability curve is overly simplistic, not accounting for known effects due to propagation or source properties. Nonetheless, the comparison suggests that the SNV and HAW hot spots do create the most high-amplitude signals observed at NVIAR (Figure 11a). The predicted HAW peak is not as sharp as the other peaks because NVIAR and Hawthorne are relatively close (∼35 km apart) and the pixel size used to create the 2D histogram is relatively large (Figure 4). The predicted hot spots to the northeast of NVIAR do not stand out in the observed detections, presumably due to propagation or source effects.

[50] Comparing the low amplitude signals to the predicted detection probability shows no correlation (Figure 11b). Instead, a sinusoidal variation exists in the observed detections with broad peaks at azimuths 90° and 270°. We interpret this to reflect enhanced detection due to seasonal reversals of zonal stratospheric winds, which has also been observed by *Le Pichon et al.* [2008, 2009]. We interpret the sharper peak between azimuths 248° (south San Jose, CA) and 263° (San Rafael, CA) to be cultural noise from the San Francisco bay area. Although the predicted detection probability is overly simplistic, the successful correlation for high amplitude events with SNV and HAW suggests that it is a useful starting point upon which additional work may improve.

5.5. Seismic Networks Versus Infrasound Arrays and the Earth Wind Filter

[51] The 400-station USArray performs well for regional infrasonic event detection. A natural follow-up question is would the 200-station Global Seismic Network perform just as well? The USArray and GSN have a station spacing of 70 and 720 km, respectively. Upon simple inspection of the detection patterns for the summer and winter events in Figure 9, one can see a rapid reduction of signal-to-noise ratio on the order of 40 dB over 600 km. The optimum record section stack (Figure 3) for the winter event shows significant energy out to 700 km. Clearly the GSN does not have the required station density to sample these infrasonic wavefronts sufficiently. However, these two signals have "B" and "C" rankings. Some of the "A" signals are observed out to 1500 km range, which spans an area that is capable of being sampled by ∼18 GSN stations. A number of the "C" events were detected out to 200 km by a comparable number of stations. Therefore, for such larger events, the GSN may have an adequate spatial density for infrasonic detection. But one important difference between stations of the USArray and GSN are the site conditions. The USArray has relatively similar site conditions whereas conditions for the GSN sites are more variable. For example, a seismometer on hard bedrock will have a smaller acoustic-to-seismic transmission coefficient than one on unconsolidated sediment. Furthermore, a seismometer in a borehole or underground shaft will not detect acoustic-to-seismic coupled signals as well as one only a meter below the surface. This variability may raise the minimum infrasonic event detection threshold that is predicted by simple scaling of USArray results.

[52] Infrasonic wind noise generated by atmospheric turbulence is a crippling problem for recording infrasound (see *Walker and Hedlin* [2010, and references therein] for a review). Wind noise is usually greatest during the day. In addition, atmospheric conditions are more favorable for long-range infrasonic event detection at night than during the day. Despite these two facts that conspire to enhance nighttime infrasonic detection, it is during the daytime that most of the infrasonic events are detected by the USArray. This suggests that USArray seismometers may be in a better position to detect and locate infrasound in the western U.S. than the handful of IMS infrasound arrays that span the North American continent. One hypothesis to explain this is that of simple coherent averaging theory; there are more seismic stations recording coherent acoustic-to-seismic coupled signal envelopes than infrasound array microphones recording local infrasonic wavefronts.

[53] An alternative hypothesis to explain the perceived improved performance of the USArray is that turbulence may not affect a seismic sensor as much as a low-frequency microphone. Spatially incoherent turbulence just above the ground does not act in phase over relatively large distances. For a non-rigid surface, a given pressure change associated

with either spatially incoherent turbulence or an infrasonic wavefront would give rise to the same seismic displacement. However, the Earth's surface is rigid; imparting a vertical displacement for a given pressure may be more efficient for infrasonic wavefronts that are spatially coherent. This hypothesis will be tested by the future USArray as it is retrofitted with three different pressure transducers designed to provide a measure of pressure from DC to 16 Hz. For both hypotheses the mechanism competes against the acoustic-to-seismic transmission coefficient. The conversion of infrasound to seismic energy is expected to be inefficient, and all other things being equal (e.g., at night when winds often cease), a higher signal-to-noise ratio is expected in microphone recordings. However, some daytime signals at the seismo-acoustic array NVIAR, at all four sites, clearly have higher signal-to-noise ratios in the 1 to 5 Hz range for the acoustic-to-seismic coupled signals recorded by the seismometers than for the pure acoustic signals recorded by the collocated microphones.

6. Conclusions

[54] Reverse time migration of infrasonic signals registered by the 2007–08 USArray, presumably due to the acoustic-to-seismic coupling phenomenon, has yielded a data set comprising 901 events that occurred in the western U.S. The optimum model parameters that best align phase-coherent seismic envelope energy along an acoustic move out velocity are source latitude, longitude, and time, as well as optimum celerity. Source altitude is ignored due to resolution limitations at the ranges spanned by the USArray. Uncertainties are provided by an automated bootstrap method and are used to separate the events into two different catalogs of 227 constrained (WUSIC-1A) and 674 unconstrained (WUSIC-1B) events.

[55] The detected events mostly occurred during the daytime and workweek and define infrasonic "hot spots" that spatially correlate with active military areas. Events at UTTR, a site where surface explosions routinely occur, are also detected and correctly located within uncertainties. The uncertainty ellipses for most events are very similar to those for the UTTR events suggesting that the average spatial accuracy is about 50 km. Source times are relatively accurate given the 100 s time sampling interval, but may be slightly biased early. The located events are interpreted to be surface explosions or sonic disturbances from brief moments of supersonic flight.

[56] To our knowledge, this work represents the first large-scale infrasonic detection and source location study using a relatively dense network of single-sensor stations that are able to fill in the gaps between globally spaced infrasonic arrays. The catalogs presented here provide first order constraints on the source parameters that explain roughly 100,000 infrasonic arrivals registered by USArray seismometers. Improvements to these parameters as well as an altitude constraint may be provided by a higher-resolution location method that can account for wind-induced velocity anisotropy, a non-point-source model, and 3-D velocity heterogeneity. Although such higher resolution catalogs can be used to statistically validate and improve propagation models, especially above the middle stratosphere where winds are not directly measured by ground-based weather stations or meteorological satellites, the WUSIC-1A catalog already provides general insights into propagation and measures of atmospheric model validation. Many of the detected events exhibit station detection patterns that suggest propagation occurred within an anisotropic stratospheric duct in the direction of the zonal stratospheric wind, which is also consistent with the predominant east-west elongated source location confidence ellipses, the Gaussian distribution of optimum celerities centered at 295 m/s, and a seasonal variation of optimum celerities that correlates at a 0.78 level with average atmospheric temperature.

[57] The success of the methods used in this study suggests that regional seismic networks near IMS infrasonic arrays may help reduce the false alarm rate by locating nearby infrasonic hot spots. The results also provide a basis for understanding infrasonic events that might be located in the western U.S. by the global IMS infrasonic network. Last, these results provide a framework for the analysis and interpretation of infrasonic recordings by microphones that will soon be integrated into the USArray.

[58] **Acknowledgments.** We want to extend a special thanks to Paul Golden for providing NVIAR infrasound data and Doug Drob for providing high-resolution mesoscale atmospheric specification models. We also thank Relu Burlacu, Roger Bowman, and Claus Hetzer for UTTR event information. Sue Nava provided information regarding mining activities in Utah, and Petru Negraru shared information about potential sources in central Nevada. Bill Phillips (Idaho Geological Survey) and Mike Stickney (Montana Bureau of Mines and Geology) provided information regarding sonic booms and mining activity in southern Idaho. The Northern California Earthquake Data Center and the University of Washington provided the locations of the quarry blasts in Oregon and Washington. The University of Wyoming Department of Atmospheric Science provided surface observations of temperature for several Nevada stations in 2007–08. The UCSD ANF team provided assistance with Antelope software. We thank Rachel Walker, Mark Zumberge, David Green, Matt Haney, Roger Waxler, and Eric Freimark for constructive comments. We also thank two anonymous reviewers and Robert Nowack for constructive reviews. This research was funded by the National Science Foundation grant EAR-1053576 and the U.S. Army Space and Missile Defense Command under contract W9113M-06-C-0029. The opinions expressed herein are those of the authors and do not necessarily reflect the views of the U.S. Army Space and Missile Defense Command.

References

Antier, K., A. Le Pichon, S. Vergniolle, C. Zielinski, and M. Lardy (2007), Multiyear validation of the NRL-G2S wind fields using infrasound from Yasur, *J. Geophys. Res.*, *112*, D23110, doi:10.1029/2007JD008462.

Arabasz, W. J., S. J. Nava, and W. T. Phelps (1997), Mining seismicity in the Wasatch Plateau and Book Cliffs mining districts, Utah, USA, in *Rockbursts and Seismicity in Mines*, edited by S. J. Gibowicz and S. Lasocki, pp. 111–116, A. A. Balkema, Rotterdam, Netherlands.

Arrowsmith, S. J., D. P. Drob, M. A. H. Hedlin, and W. Edwards (2007), A joint seismic and acoustic study of the Washington State bolide: Observations and modeling, *J. Geophys. Res.*, *112*, D09304, doi:10.1029/2006JD008001.

Arrowsmith, S. J., M. A. Hedlin, B. Stump, and M. D. Arrowsmith (2008), Infrasonic signals from large mining explosions, *Bull. Seismol. Soc. Am.*, *98*, 768–777, doi:10.1785/0120060241.

Bahavar, M., et al. (2007), Enhanced resources of the SMDC monitoring research program for source information and data acquisition, paper presented at the 29th Monitoring Research Review: Ground-Based Nuclear Explosion Monitoring Technologies, Natl. Nucl. Security Admin., Denver, Colo.

Baldwin, M. P., and T. J. Dunkerton (1999), Propagation of the Arctic Oscillation from the stratosphere to the troposphere, *J. Geophys. Res.*, *104*, 30,937–30,946, doi:10.1029/1999JD900445.

Blanc-Benon, P., B. Lipkens, M. F. Hamilton, and D. T. Blackstock (2002), Propagation of finite amplitude sound through turbulence: Modeling with geometrical acoustics and the parabolic approximation, *J. Acoust. Soc. Am.*, *111*, 487–498, doi:10.1121/1.1404378.

Busby, R. W., F. L. Vernon, R. L. Newman, and L. Astiz (2006), EarthScope's USArray: Advancing eastward, *Eos Trans. AGU*, *87*(52), Fall Meet. Suppl., Abstract U41B-0820.

Cansi, Y. (1995), An automated seismic event processing for detection and location: The P.M.C.C. method, *Geophys. Res. Lett.*, *22*, 1021–1024, doi:10.1029/95GL00468.

Christie, D. R., and P. Campus (2010), The IMS infrasound network: Design and establishment of infrasound stations, in *Infrasound Monitoring for Atmospheric Studies*, edited by A. Le Pichon, E. Blanc, and A. Hauchecorne, pp. 29–75, Springer, New York, doi:10.1007/978-1-4020-9508-5_2.

Claerbout, J. F. (1971), Toward a unified theory of reflector mapping, *Geophysics*, *36*, 467–481, doi:10.1190/1.1440185.

Cochran, E., and P. Shearer (2006), Infrasound events detected with the Southern California Seismic Network, *Geophys. Res. Lett.*, *33*, L19803, doi:10.1029/2006GL026951.

Craig, R. A., and W. S. Hering (1959), The stratospheric warming of January-February 1957, *J. Meteorol.*, *16*, 91–107, doi:10.1175/1520-0469(1959)016<0091:TSWOJF>2.0.CO;2.

de Groot-Hedlin, C. D. (2008), Finite difference time domain synthesis of infrasound propagation through an absorbing atmosphere, *J. Acoust. Soc. Am.*, *124*, 1430–1441, doi:10.1121/1.2959736.

de Groot-Hedlin, C. D., M. A. H. Hedlin, K. T. Walker, D. D. Drob, and M. A. Zumberge (2008), Evaluation of infrasound signals from the shuttle Atlantis using a large seismic network, *J. Acoust. Soc. Am.*, *124*, 1442–1451, doi:10.1121/1.2956475.

de Groot-Hedlin, C. D., M. A. H. Hedlin, and D. Drob (2010), Atmospheric variability and infrasound monitoring, in *Infrasound Monitoring for Atmospheric Studies*, edited by A. Le Pichon, E. Blanc, and A. Hauchecorne, pp. 475–507, Springer, New York, doi:10.1007/978-1-4020-9508-5_15.

de Groot-Hedlin, C., M. Hedlin, and K. Walker (2011), Finite difference synthesis of infrasound propagation through a windy, viscous atmosphere: Application to a bolide explosion detected by seismic networks, *Geophys. J. Int.*, *185*, 305–320, doi:10.1111/j.1365-246X.2010.04925.x.

Drob, D. P., J. M. Picone, and M. Garceés (2003), Global morphology of infrasound propagation, *J. Geophys. Res.*, *108*(D21), 4680, doi:10.1029/2002JD003307.

Drob, D. P., M. M. Garceés, M. A. Hedlin, and N. Brachet (2010), The temporal morphology of infrasound propagation, *Pure Appl. Geophys.*, *167*, 437–453, doi:10.1007/s00024-010-0080-6.

Edwards, W. N., and A. R. Hildebrand (2004), SUPRACENTER: Locating fireball terminal bursts in the atmosphere using seismic arrivals, *Meteorit. Planet. Sci.*, *39*, 1449–1460, doi:10.1111/j.1945-5100.2004.tb00121.x.

Efron, B., and R. J. Tibshirani (1993), *An Introduction to the Bootstrap*, *Monogr. on Stat. and Appl. Probab.*, vol. 57, Chapman and Hall, New York.

Ekström, G., M. Nettles, and G. A. Abers (2003), Glacial earthquakes, *Science*, *302*, 622–624, doi:10.1126/science.1088057.

Evers, L. G., and H. W. Haak (2010), The characteristics of infrasound, its propagation and some early history, in *Infrasound Monitoring for Atmospheric Studies*, edited by A. Le Pichon, E. Blanc, and A. Hauchecorne, pp. 3–27, Springer, New York, doi:10.1007/978-1-4020-9508-5_1.

Evers, L. G., and P. Siegmund (2009), Infrasonic signature of the 2009 major sudden stratospheric warming, *Geophys. Res. Lett.*, *36*, L23808, doi:10.1029/2009GL041323.

Garceés, M. (2004), On using ocean swells for continuous infrasonic measurements of winds and temperature in the lower, middle, and upper atmosphere, *Geophys. Res. Lett.*, *31*, L19304, doi:10.1029/2004GL020696.

Gibson, R. G., D. P. Drob, D. Broutman, and N. W. Winslow (2010), Advancement of techniques for modeling the effects of atmospheric gravity-wave-induced inhomogeneties on infrasound propagation, paper presented at the 32nd Monitoring Research Review: Ground-Based Nuclear Explosion Monitoring Technologies, Natl. Nucl. Security Admin., Orlando, Fla.

Green, D. N., and D. Bowers (2010), Estimating the detection capability of the International Monitoring System infrasound network, *J. Geophys. Res.*, *115*, D18116, doi:10.1029/2010JD014017.

Gutenberg, B. (1939), The velocity of sound waves and the temperature in the stratosphere in southern California, *Bull. Am. Meteorol. Soc.*, *20*, 192–201.

Hagerty, M. T., W.-Y. Kim, and P. Martysevich (2002), Infrasound detection of large mining blasts in Kazakstan, *Pure Appl. Geophys.*, *159*, 1063–1079, doi:10.1007/s00024-002-8673-3.

Haney, M. M. (2009), Infrasonic ambient noise interferometry from correlations of microbaroms, *Geophys. Res. Lett.*, *36*, L19808, doi:10.1029/2009GL040179.

Hedlin, M. A. H., D. Drob, K. Walker, and C. de Groot-Hedlin (2010), A study of acoustic propagation from a large bolide in the atmosphere with a dense seismic network, *J. Geophys. Res.*, *115*, B11312, doi:10.1029/2010JB007669.

Ishihara, Y., S. Tsukada, S. Sakai, Y. Hiramatsu, and M. Furumoto (2003), The 1998 Miyako fireball's trajectory determined from shock wave records of a dense seismic array, *Earth Planets Space*, *55*, 9–12.

Kallistratova, M. A. (2002), Acoustic waves in the turbulent atmosphere: A review, *J. Atmos. Oceanic Technol.*, *19*, 1139–1150, doi:10.1175/1520-0426(2002)019<1139:AWITTA>2.0.CO;2.

Kanamori, H., J. Mori, D. L. Anderson, and T. Heaton (1991), Seismic excitation by the space shuttle Columbia, *Nature*, *349*, 781–782, doi:10.1038/349781a0.

Kappus, M., and F. L. Vernon (1991), Acoustic signature of thunder from seismic records, *J. Geophys. Res.*, *96*, 10,989–11,006, doi:10.1029/91JD00789.

Kulichkov, S. N. (2008), Evidence for nonlinear atmospheric effects in infrasound propagation from explosions of different types and yields, paper presented at Nonlinear Acoustics—Fundamentals and Applications: 18th International Symposium, Nonlinear Acoust. Soc. of Jpn., Stockholm.

Kulichkov, S. N., I. P. Chunchuzov, and O. I. Popov (2010), Simulating the influence of an atmospheric fine inhomogeneous structure on long range propagation of pulsed acoustic signals, *Izv. Russ. Acad. Sci. Atmos. Oceanic Phys., Engl. Transl.*, *46*, 60–68, doi:10.1134/S0001433810010093.

Landau, L. D., and E. M. Lifshitz (1959), *Fluid Mechanics: Course of Theoretical Physics*, *Addison-Wesley Ser. in Adv. Phys.*, vol. 6, Pergamon, London.

Langston, C. A. (2004), Seismic ground motions from a bolide shock wave, *J. Geophys. Res.*, *109*, B12309, doi:10.1029/2004JB003167.

Le Pichon, A., J. Vergoz, P. Herry, and L. Ceranna (2008), Analyzing the detection capability of infrasound arrays in central Europe, *J. Geophys. Res.*, *113*, D12115, doi:10.1029/2007JD009509.

Le Pichon, A., J. Vergoz, E. Blanc, J. Guilbert, L. Ceranna, L. Evers, and N. Brachet (2009), Assessing the performance of the International Monitoring System's infrasound network: Geographical coverage and temporal variabilities, *J. Geophys. Res.*, *114*, D08112, doi:10.1029/2008JD010907.

Lingevitch, J. F., M. D. Collins, and W. L. Siegmann (1999), Parabolic equations for gravity and acousto-gravity waves, *J. Acoust. Soc. Am.*, *105*, 3049–3056, doi:10.1121/1.424634.

McKenna, M. H., B. W. Stump, S. Hayek, J. R. McKenna, and T. R. Stanton (2007), Teleinfrasonic studies of hard-rock mining explosions, *J. Acoust. Soc. Am.*, *122*, 97–106, doi:10.1121/1.2741375.

McKenna, M. H., B. W. Stump, and C. Hayward (2008), Effect of time-varying tropospheric models on near-regional and regional infrasound propagation as constrained by observational data, *J. Geophys. Res.*, *113*, D11111, doi:10.1029/2007JD009130.

McMechan, G. A. (1983), Migration by extrapolation of time-dependent boundary values, *Geophys. Prospect.*, *31*, 413–420, doi:10.1111/j.1365-2478.1983.tb01060.x.

Negraru, P. T., P. Golden, and E. T. Herrin (2010), Infrasound propagation in the "Zone of Silence", *Seismol. Res. Lett.*, *81*, 614–624, doi:10.1785/gssrl.81.4.614.

Qamar, A. (1995), Space shuttle and meteoroid-tracking supersonic objects in the atmosphere with seismographs, *Seismol. Res. Lett.*, *66*, 6–12, doi:10.1785/gssrl.66.5.6.

Richins, W. D. (1979), Data processing and analysis, in *Earthquake Studies in Utah 1850 to 1978: Special Publication of the University of Utah Seismographic Stations*, edited by W. J. Arabasz, R. B. Smith, and W. D. Richins, pp. 79–90, Univ. of Utah, Salt Lake City.

Shearer, P. (1994), Global seismic event detection using a matched filter on long-period seismograms, *J. Geophys. Res.*, *99*, 13,713–13,725, doi:10.1029/94JB00498.

Sorrells, G. G., E. T. Herrin, and J. L. Bonner (1997), Construction of regional ground truth databases using seismic and infrasound data, *Seismol. Res. Lett.*, *68*, 743–752, doi:10.1785/gssrl.68.5.743.

Stolt, R. H. (1978), Migration by Fourier transform, *Geophysics*, *43*, 23–48, doi:10.1190/1.1440826.

Stump, B. W., M. H. Hedlin, D. C. Pearson, and V. Hsu (2002), Characterization of mining explosions at regional distances: Implications with the International Monitoring System, *Rev. Geophys.*, *40*(4), 1011, doi:10.1029/1998RG000048.

Sutherland, L. C., and H. E. Bass (2004), Atmospheric absorption in the atmosphere up to 160 km, *J. Acoust. Soc. Am.*, *115*, 1012–1032, doi:10.1121/1.1631937.

Vernon, F. L., M. A. Hedlin, R. W. Busby, and R. Woodward (2010), Observing infrasound and atmospheric pressure with the NSF EarthScope USArray, Abstract S11A-1920 presented at 2010 Fall Meeting, AGU, San Francisco, Calif., 13–17 Dec.

Walker, K. T., and M. A. H. Hedlin (2010), A review of wind noise reduction methodologies, in *Infrasound Monitoring for Atmospheric Studies*, edited by A. Le Pichon, E. Blanc, and A. Hauchecorne, pp. 141–182, Springer, New York, doi:10.1007/978-1-4020-9508-5.

Walker, K. T., M. A. H. Hedlin, C. de Groot-Hedlin, J. Vergoz, A. Le Pichon, and D. P. Drob (2010), Source location of the 19 February 2008 Oregon bolide using seismic networks and infrasound arrays, *J. Geophys. Res.*, *115*, B12329, doi:10.1029/2010JB007863.

Wang, L., and M. J. Alexander (2009), Gravity wave activity during stratospheric sudden warmings in the 2007–2008 Northern Hemisphere winter, *J. Geophys. Res.*, *114*, D18108, doi:10.1029/2009JD011867.

West, M., K. E. Gilbert, and R. A. Sack (1992), A tutorial on the parabolic equation (PE) model used for long range propagation in the atmosphere, *Appl. Acoust.*, *37*, 31–49, doi:10.1016/0003-682X(92)90009-H.

C. de Groot-Hedlin, M. A. H. Hedlin, R. Shelby, F. Vernon, and K. T. Walker, Institute of Geophysics and Planetary Physics, Scripps Institution of Oceanography, University of California, San Diego, La Jolla, CA 92093, USA. (kwalker@ucsd.edu)